ISET Journal of Earthquake Technology, Paper No. 415, Vol. 39, No. 1-2, March-June 2002, pp. 1-19

NON-LINEAR RESPONSE AND MODELLING OF RC WALLS SUBJECTED TO SEISMIC LOADING

N. Ile, J.M. Reynouard and J.F. Georgin
20 Av. Albert Einstein, URGC-Structures
INSA-Lyon, Bât 304, 69100 Villeurbanne, France

ABSTRACT

In this paper, attention is focused on the modelling of the seismic response of RC walls with different reinforcement ratios. A numerical investigation is carried out with reference to three different specimens, whose measured seismic responses were obtained by other authors. For each specimen, an interpretation of the experimental results is attempted through a finite element non-linear cyclic model. A concrete model including a smeared cracking capability is used, which allows the sequence of crack opening and propagation through the shear wall specimens to be followed. Although the walls have the same geometry, their seismic behaviour and final failure mode are affected by the reinforcement ratio and detailing provisions. Some of the parameters and mechanisms which significantly influenced the specimens response are described. Knowledge gained from this study is important in understanding the behaviour of RC walls under earthquake loading and will help development of earthquake-resistant design.

KEYWORDS: R/C Wall, Seismic Loading, Plane Stress, Finite Element Analysis

INTRODUCTION

Due to the fact that structural walls are used extensively in moderate and high-rise buildings, the seismic performance of many structural systems is closely related to the behaviour of reinforced concrete walls. Since the application of simplified procedures used for design gives limited insight into the real seismic response of a wall structure, design and vulnerability evaluation may become increasingly dependent on response predictions based on finite element analyses using non-linear models. On one hand, the calculations based on non-linear models can give a more realistic estimation of the displacement and ductility demand and of the damage distribution of this type of structural member. On the other hand, the principal shortcoming of this tool is the lack of common rules of utilisation and the fact that there are no generally accepted mathematical models for reinforced concrete members. If the method is to become a useful part of the design and seismic assessment of existing buildings, a strong interaction between experimental and numerical results is required. The accuracy and efficiency of the computational tools in predicting the seismic response of wall structures can be verified in a systematic way if measured responses of scale RC wall structures tested on shaking table are available. In this case, comparing numerical and experimental results gives a great help in calibrating the numerical models and in understanding the behaviour of the test specimens more clearly.

In the past two decades, extensive experimental and analytical research on the seismic behaviour of RC wall structures has been conducted mainly in the USA, Japan, New Zealand and Europe. Sophisticated material models have been implemented, and various approaches have been proposed to predict the inelastic response of RC structural walls (ASCE, 1982; Vulcano et al., 1988). Nearly all these experimental and analytical studies have concentrated on the seismic behaviour of walls designed and detailed to develop a ductile flexural plastic hinge only at the base. Very little attention has been paid to the seismic behaviour of lightly reinforced RC walls.

RC bearing walls with limited reinforcement ratios are commonly used in France for the building structures. In this kind of structures, as masonry is generally not used for partitioning, walls arrangement is redundant when compared to the structural demand (Bisch and Coin, 1998). If applied to this kind of wall structures, code provisions for ductile walls may lead to very expensive solutions and unnecessary overstrength. An alternative design procedure may be adopted, if instead of "localizing" damage at the base, the wall can be allowed to go inelastic and develop cracking and/or plastic hinges at any location

along its height. Because, in this approach, damage is intended to be distributed over the height of the structure, this approach has also been called as the "multi-fuse" concept (Mazars, 1998).

Slender walls may be designed in this way as lightly reinforced walls, the flexural reinforcement being curtailed in accordance with the bending moment diagram. Besides the lower costs corresponding to the limited reinforcement ratio, this technique seems to be able to ensure an adequately seismic behaviour. In such kind of structures, earthquake energy is dissipated along the wall height by means of reinforcement yielding and inelastic behaviour of concrete. However, if flexural behaviour is preponderant, the seismic energy injected in the structure is also partly balanced by the rising of masses due to the normal cracking of sections and eventual uplift of foundations.

During the current conversion of Eurocode 8 into a standard (EN1998-1: Design of structures for earthquake resistance), "large lightly reinforced walls" have been introduced along with the ductile walls present in the ENV (prestandard) version of EC 8, (Fardis, 2000). Within the French CAMUS (Bisch and Coin, 1998) and European TMR (Training and Mobility of Researchers) projects [www.cordis.lu/tmr/home.html), three RC wall specimens were subjected to shaking table tests, with a large number of interesting results. The first two specimens were lightly reinforced and were designed following the French PS92 seismic code. The third specimen was designed following the EC8 and much more reinforcement was needed to comply with this code's capacity design principles.

Several interesting aspects of the seismic behaviour of lightly reinforced walls have been clarified by the experimental work and subsequent numerical studies associated with the CAMUS research programme. By comparing experimental and non-linear numerical results, interest in this investigation is focused on the understanding of the most important factors that may affect the seismic behaviour and failure mechanism of RC walls with different reinforcement ratios, ranging from lightly or very lightly to normally reinforced walls.

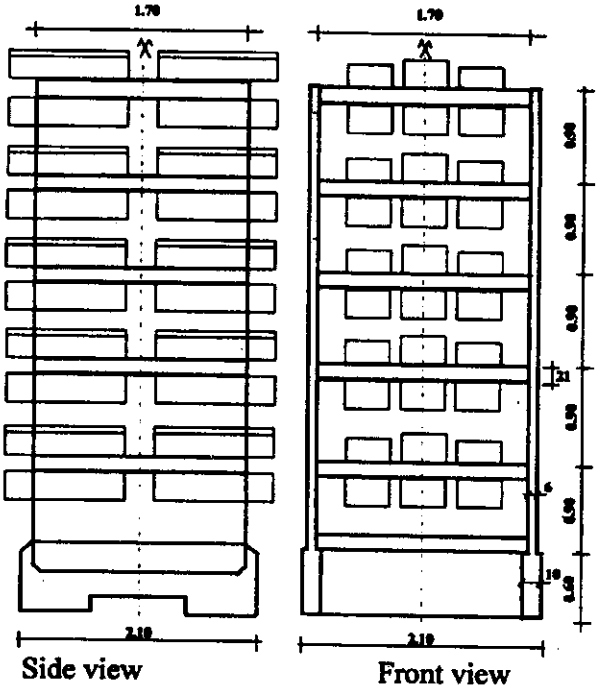

Fig. 1 General scheme of the CAMUS specimens

THE ANALYSED STRUCTURES: GEOMETRY AND DESIGN

Three different specimens with different reinforcement ratios which were tested on the shaking table of CEA-Saclay have been analysed. The three structures (CAMUS I, CAMUS II and CAMUS III) have the same geometrical dimensions. Each specimen consists of a 1/3 scaled model, composed of two parallel 5-floor RC walls without openings, linked together by 6 square floors, and the reinforced concrete footing being anchored to the shaking table (Figure 1). The walls are each 5.10 m height, 1.70 m long and

6 cm thick. They were cast in order to reproduce the construction joints at the level of each floor. All the floors are 1.70 m long, 1.70 m wide and 21 cm thick. The wall footing is 2.10 m wide, 0.60 m high and 10 cm thick. Additional mass was added to the upper and lower parts of each floor (excepting the first floor) in order to simulate the gravity load compatible with the vertical stress values commonly found at the base of this type of structure (about 1.6 MPa). A bracing system aiming at stabilising the structure in the direction perpendicular to the walls was installed at each storey. Its design is such that it does not interfere with the in-plane flexural behaviour of the walls, only horizontal perpendicular forces being transferred to it.

The first two specimens have been designed and detailed according to the French PS 92 seismic code. Their general characteristics have been deduced from elements which can be currently found in a real building. Design of the first specimen, CAMUS I has been carried out so that, at least the three lower storeys have the necessary rebars to reach the flexural capacity of the sections (Coin, 1998). To enforce a predominantly flexural behaviour with nearly horizontal cracking, the reinforcement ratio changes between two storeys in order to obtain steel yielding at several storeys and not a concentrated plastic hinge in the lower part of the wall. To comply with the verification of sliding shear, a vertical reinforcement was placed in the centre of the wall, in addition to that required for flexural resistance. Figure 2(a) gives the steel bars at each storey for the first specimen. The positions of the interruption of steel bars and the construction joint are shown in Figure 3.

Following the same design concepts, the second model CAMUS II has been designed for a minimal reinforcement resisting to flexure so that only at the first storey, the rebars contribute to the flexural capacity, while the upper storeys could behave without any reinforcement (Coin, 1998). Figure 2(b) shows the reinforcement for the second specimen.

According to PS92 code, to prevent shear failure and in recognition of the fact that the shear behaviour factor is not the same as that corresponding to the flexural behaviour, design shear forces are increased to about double the seismic shear forces from analysis. This is taken into account by magnifying the shear force obtained from analysis by the factor $q' = (q+1)/2$. Verification under shear force of the CAMUS I and II specimens indicated that the amplified designed shear is less than the design shear strength without reinforcement, so the two specimens have no horizontal shear reinforcement (Figure 2). With a PS92 specified seismic action defined by the NICE S1 PS92 design spectrum, the first specimen has been designed for a peak ground acceleration (PGA) of about 0.96g and to a behaviour factor q = 3.06. For the second specimen, the design PGA is about 0.52g, corresponding to a behaviour factor q = 3.79.

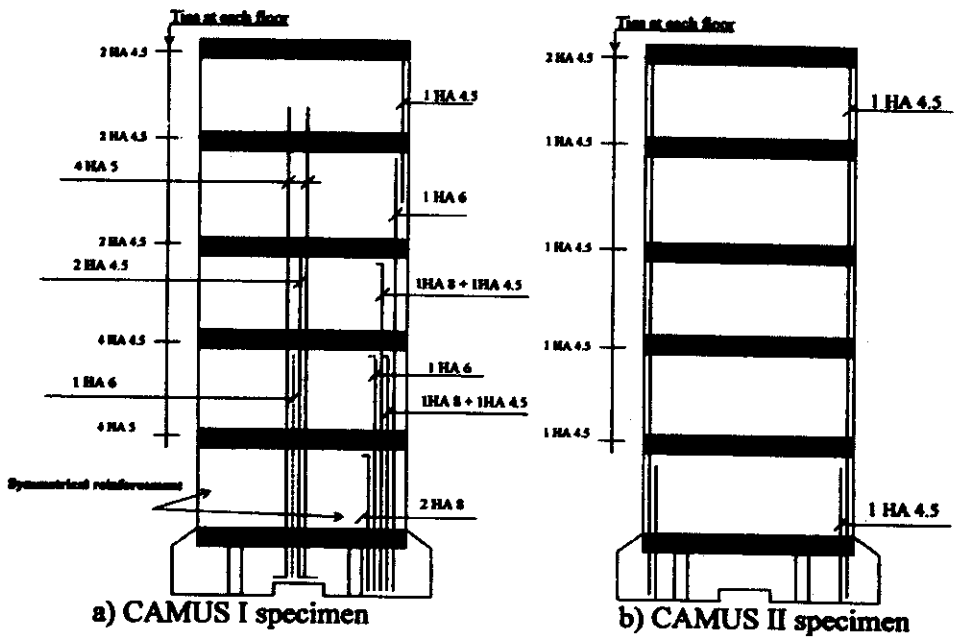

Fig. 2 Steel reinforcement of the CAMUS I and II specimens

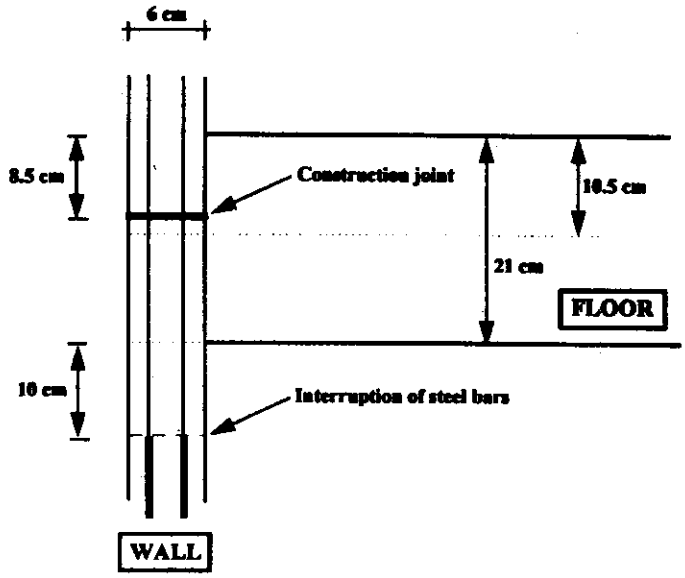

Fig. 3 Interruption of steel and position of the construction joint for CAMUS I

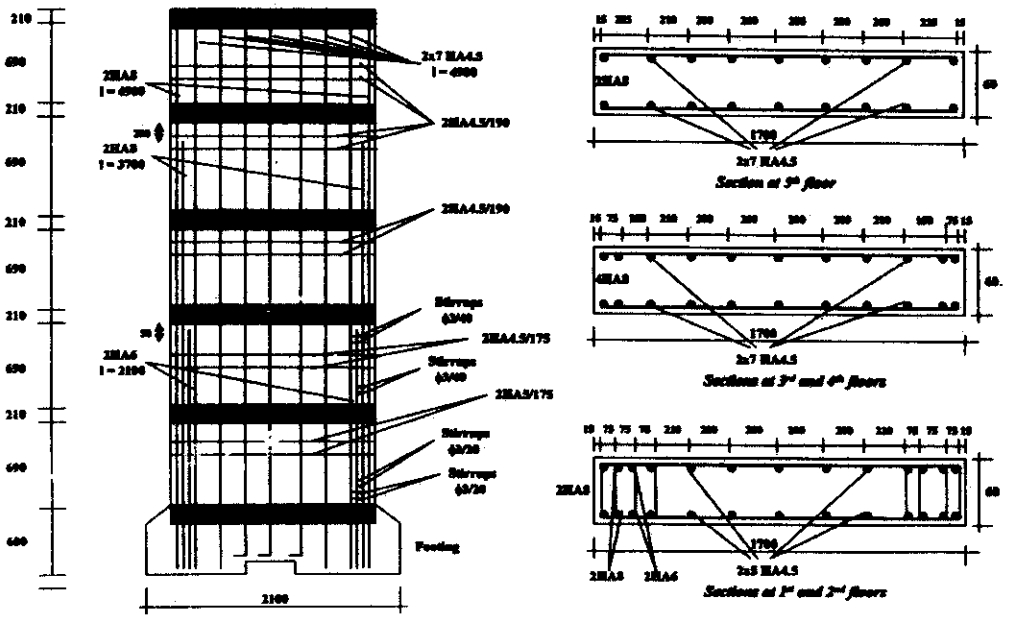

Fig. 4 Steel reinforcement of CAMUS III specimen

The last specimen CAMUS III has been designed and detailed in accordance with EC 8 requirements. Although the ultimate bending moment is the same as that corresponding to the first specimen, CAMUS III was designed and detailed to develop a ductile flexural plastic hinge only at the base (Cafeel, 2001). Above the base region, the wall was overdesigned in flexure to avoid development of inelasticity anywhere over the height, and designed shear forces were well above those corresponding to flexural plastic hinging at the base. The PGA corresponding to the flexural capacity is about 0.785g and the nominal q-factor according to EC8, is equal to about 2.7. The steel reinforcement and the drawings of 3 sections of CAMUS III specimen are given in Figure 4. The differences in reinforcement between CAMUS I and III concern mainly the shear reinforcement and vertical reinforcement in the upper storeys. Table 1 presents a comparison between the longitudinal reinforcement of CAMUS I and III. Tables 2 and 3 show the main characteristics of the steel reinforcement, which was used in the construction of the specimens.

Table 1: Longitudinal Reinforcement of the CAMUS I and III Specimens

	Boundaries (CAMUS I)	Boundaries (CAMUS III)	Central reinforcement (CAMUS I)	Central reinforcement (CAMUS III)
1st st..	4ϕ8+2ϕ6+2ϕ4.5=289mm^2	4ϕ8+2ϕ6+2ϕ4.5=289mm^2	4ϕ5+2ϕ4.5+ϕ6=138mm^2	2x5ϕ4.5/200=159mm^2
2nd st.	4ϕ6+2ϕ8+2ϕ4.5=189mm^2	4ϕ8+2ϕ6+2ϕ4.5=289mm^2	4ϕ5+2ϕ4.5+ϕ6=138mm^2	2x5ϕ4.5/200=159mm^2
3rd st.	ϕ6+ϕ8+ϕ4.5=94.4mm^2	4ϕ8+2ϕ4.5=233mm^2	4ϕ5+2ϕ4.5=110mm^2	2x5ϕ4.5/200=159mm^2
4th st.	ϕ6=28.2mm^2	4ϕ8+2ϕ4.5=233mm^2	4ϕ5=78.4mm^2	2x5ϕ4.5/200=159mm^2
5th st.	ϕ4.5=15.9mm^2	2ϕ8+2ϕ4.5=132mm^2	4ϕ5=78.4mm^2	2x5ϕ4.5/200=159mm^2

Table 2: Main Material Characteristics of the Steel Reinforcement for CAMUS I and II

ϕ (mm)	f_{sy} (MPa)	f_{su} (MPa)	ϵ_{su} (%)
4.5	465	520	2.5
5	570	605	2.5
6	515	565	5.5
8	430	455	5.0

Table 3: Main Material Characteristics of the Steel Reinforcement for CAMUS III

ϕ (mm)	f_{sy} (MPa)	f_{su} (MPa)	ϵ_{su} (%)
4.5	563	581	2.18
5	631	646	0.93
6	593	625	3.38
8	486	587	16.8

f_{sy} - yield strength

f_{su} - tensile failure strength

ϵ_{su} - strain at failure

The concrete material characteristics were measured from tests on cylinders of the same concrete as the specimens. The results of the tests indicated the following average values for the concrete compressive strength (f_c') and the Young's modulus (E_{cr}):

CAMUS I: $f_c' = 35$ MPa, $E_{cr} = 30\,650$ MPa

CAMUS II: $f_c' = 26$ MPa, $E_{cr} = 25\,000$ MPa

CAMUS III : $f_c' = 39$ MPa, $E_{cr} = 31\,140$ MPa

SEISMIC ACTION

During the shaking table tests, the specimens were subjected to increasing horizontal accelerations along the direction parallel to the walls' plane. The main part of the tests has been performed with an artificial accelerogram named Nice, generated to fit the French PS92 elastic spectrum, which is

representative of a far-field earthquake. In order to study the seismic response of the specimens subjected to a near-field type of excitation, two recorded signals named San Francisco and Melendy Ranch have also been used for intermediate tests on the specimens CAMUS I and III. These signals are characteristics of near-field earthquakes (important acceleration but short duration and different frequency content). Before the test, an extensive parametric study was performed with a non-linear fibre-type model (Combescure et al., 1998) in order to compare the effects of both types of signals and to decide the level of excitation to be applied during the test. For each specimen, the seismic tests' sequence was as follows:

CAMUS I: Nice 0.24g, San Francisco 1.11g, Nice 0.24g, Nice 0.40g, Nice 0.71g
CAMUS II: Nice 0.10g, Nice 0.23g, Nice 0.52g, Nice 0.51g
CAMUS III: Nice 0.42g, Nice 0.22g, Melendy Ranch 1.35g, Nice 0.64g, Nice 1.0g

Due to the heavy demands on computer time, the finite element analysis considered only two input motions for each test. In this partial representation of the real test sequence, the applied accelerograms are the ones which have caused the most significant damage to the specimens. In combination with the ability of code CASTEM 2000 to save the damage state after each analysis, the following sequence was considered in chronological order in each case:

Nice 0.40g and Nice 0.71g for CAMUS I,
Nice 0.51g and Nice 0.51g for CAMUS II and
Nice 0.42g and Melendy Ranch 1.35g for CAMUS III.

It is to be noted that one of the aims of the present study was to test the predictive capabilities of the numerical analysis at failure or close to failure. Therefore, the numerical results and comparison with measured values are related only to the following applied motions for each specimen: Nice 0.71g for CAMUS I, Nice 0.51g for CAMUS II and Melendy Ranch 1.35g for CAMUS III.

The Nice (0.71g) and Melendy Ranch (1.35g) as well as their corresponding acceleration response spectra are shown in Figures 5(a) and 5(b).

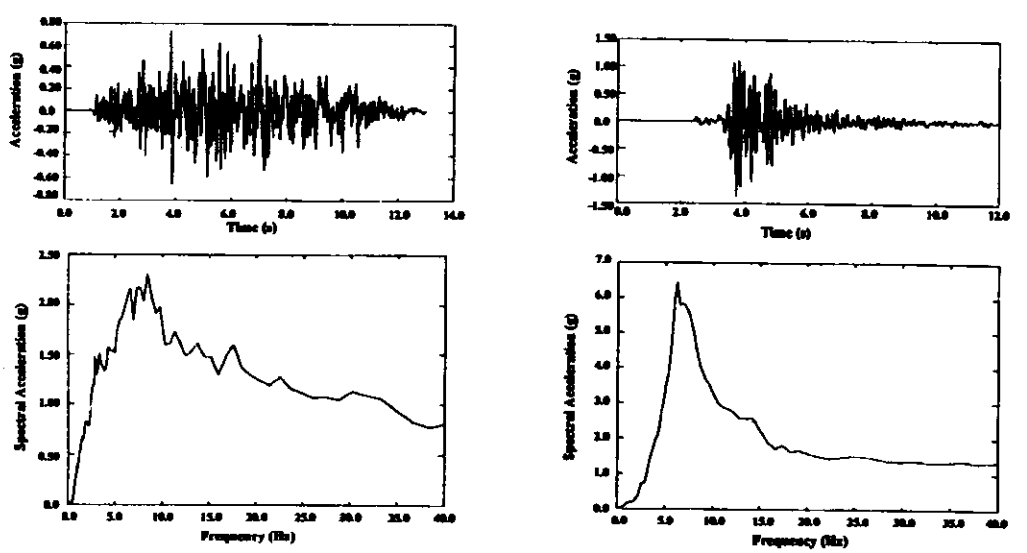

a) Nice signal (a_{max} = 0.71g) b) Melendy Ranch signal (a_{max} = 1.35g)

Fig. 5 Input signals and acceleration spectra (5% damping)

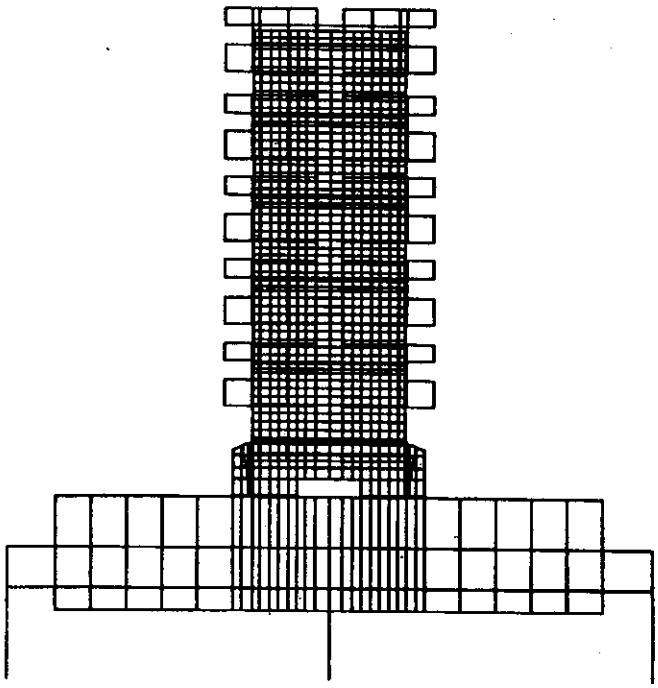

Fig. 6 2-D finite element mesh of the CAMUS specimens including the shaking table

MODELLING APPROACH AND EIGENFREQUENCY ANALYSIS

The numerical analyses have been performed using the general purpose finite element program CASTEM 2000 developed at CEA-Saclay (Millard, 1993). To predict the inelastic seismic response of the tested structures with sufficient accuracy, due care has been given to create detailed models of the specimens, taking into account the necessary geometric characteristics, construction details and boundary conditions. The specimens were assumed to be in a state of plane stress, and half of the wall specimens were represented on account of the symmetry in geometry and loading. Figure 6 shows the global 2-D finite element mesh, and Figures 7(a), 7(b) and 7(c) present its different parts adopted for each case under analysis.

The 2-D finite element model represents the different parts of the mock-up and the shaking-table as an equivalent plane mesh. Four-node membrane elements were used to represent the wall, the slabs, the additional mass and the shaking table. In the case of CAMUS II specimen, double nodes were provided from the beginning along the concrete inter-element boundaries at the level of the cold construction joints, and unilaterally imposed kinematic conditions were considered in these locations. This formulation was intended to represent more accurately the multi-bloc character of the dynamic system induced by the very low reinforcement ratio. The shaking-table was considered as a rigid block fixed to 4 vertical restraining rods: 2 rods situated at the level of the centre of the wall and the other two at the extremities (the axial stiffness of each rod being estimated equal to 400 MN/m). A discrete modelling was adopted to represent the reinforcement through the use of two-node truss elements. Perfect bond between steel bars and concrete was considered for CAMUS I and CAMUS III specimens. However, because smooth reinforcing bars were used for CAMUS II specimen, bond-slip interaction between steel bars and concrete was explicitly modeled in this case through the use of four-node continuous contact elements.

Non-linear inelastic behaviour was assumed for the entire wall structure (concrete, steel and interface elements), while the behaviour of the finite elements representing the slabs, the additional mass and the shaking table was taken as elastic.

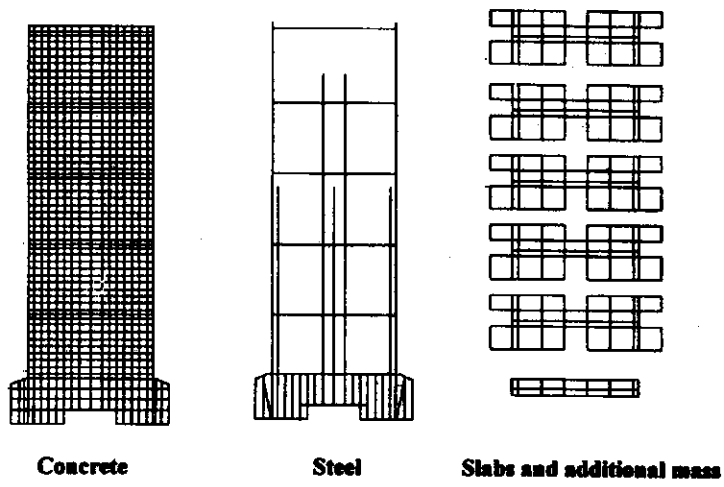

(a) CAMUS I wall specimen

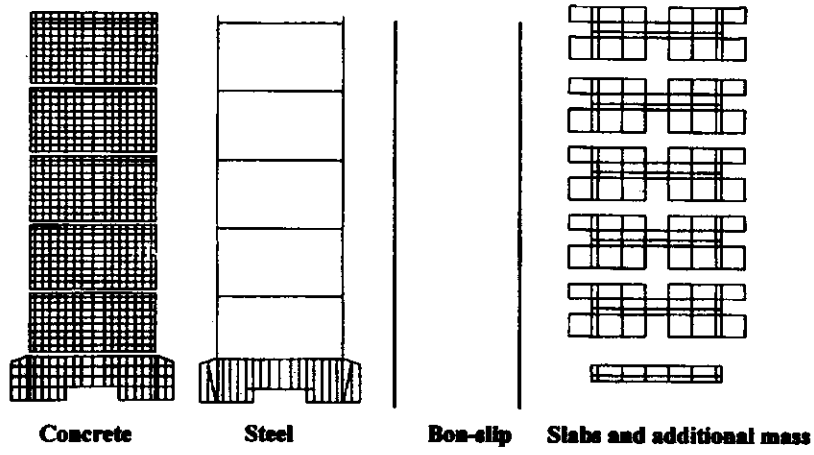

(b) CAMUS II wall specimen

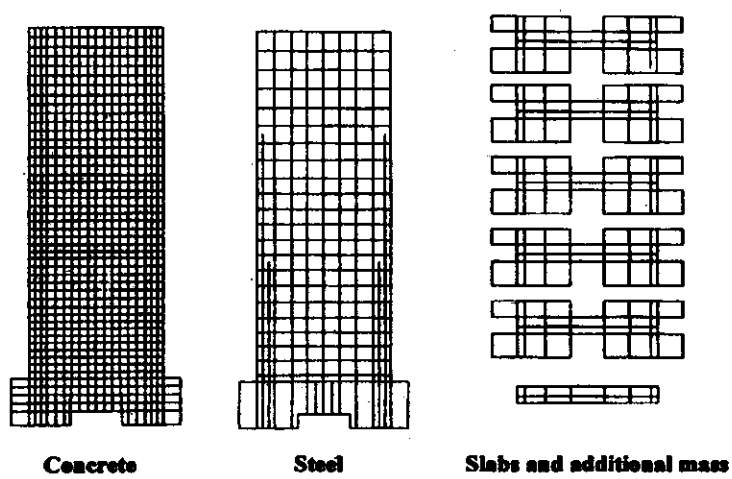

(c) CAMUS III wall specimen

Fig. 7 Constituent elements of the finite element mesh for CAMUS wall specimens

For reasons of validation of the modeling assumptions, eigenvalue analyses were performed for each of the finite element models. Elastic material properties were used, taking Young's modulus for concrete as 30,000 MPa for CAMUS I and III and 25,000 MPa for CAMUS II, respectively. Two different situations were considered corresponding to the assumptions of perfectly-fixed (rigid) and elastic contact between the wall footing and the shaking-table. To model the elastic contact between the specimen and the shaking-table, a 1 cm thick four-node finite element layer was introduced at the base of the wall footing having an elastic behaviour with a modulus of elasticity E_c. The reason for this modeling approach was based on the experimentally observed relative vertical movements between the base of the wall footing and the shaking table, which appeared even for very low seismic motions. Therefore, different values for the elastic modulus E_c were selected in order to have a good match of the first natural frequencies of the test specimens. Tables 4, 5 and 6 present the values of the first two natural frequencies confronted with the test results. The 1st natural frequency corresponds to the flexural vibration mode of the specimen, while the 2nd natural frequency corresponds to the vertical vibration of the combined system (specimen and shaking-table). As shown in the tables, the frequency values based on the assumption of elastic contact between the base of the specimen and the shaking-table agree reasonably well with the measured values. Therefore, the elastic contact assumption was adopted for simulating the inelastic time-history response of the CAMUS specimens.

Table 4: Values of the Natural Frequencies for CAMUS I

NATURAL FREQUENCY (Hz)			
	rigid contact	**elastic contact (E_c=3000 MPa)**	**test**
1st (longitudinal)	8.50	7.27	7.24
2nd (vertical)	28.30	22.34	20.00

Table 5: Values of the Natural Frequencies for CAMUS II

NATURAL FREQUENCY (Hz)			
	rigid contact	**elastic contact (E_c=1400 MPa)**	**test**
1st (longitudinal)	8.26	6.13	6.4
2nd (vertical)	22.98	20.81	19.00

Table 6: Values of the Natural Frequencies for CAMUS III

NATURAL FREQUENCY (Hz)			
	rigid contact	**elastic contact (E_c=1400 MPa)**	**test**
1st (longitudinal)	9.15	6.85	6.9
2nd (vertical)	23.63	22.01	19.00

Assuming a 2% critical damping factor (close to the measured damping value) for the first vibration mode, and 1% for the second mode (because usually higher modes are less damped), the damping parameters α and β were calculated and used subsequently to form the Rayleigh damping matrix $[C]=\alpha[M]+\beta[K]$, M and K being the mass and stiffness matrix. Despite the fact that a modal characterisation is theoretically correct only for linear elastic systems, the damping matrix $[C]$ obtained in this way is assumed to remain constant throughout the loading cycle. Since with increasing damage, modal frequencies decrease due to cracking and reinforcement yielding, this assumption may lead to unrealistic overdamping on lower modes. When several sequential input motions are considered in a seismic analysis, the best choice would probably be to reduce the Rayleigh damping matrix with increasing applied motion. The drawback of this approach relies on the difficulty of selecting a suitable value for the damping matrix. Notwithstanding the complexity of the problem, it seems, however, that the

viscous overdamping effect may be partially compensated by the fact that the present non-linear model cannot take properly into account all sources of hysteretic damping: unilateral cracking, shear slip between the lips of the crack, bond-slip between steel and concrete, etc. In any case, since one of the aims of the present study was to test the capabilities of the existing cyclic model, all modelling decisions (including the choice of a constant damping matrix) were made before all calculations were executed and no tuning of the analysis was done in an attempt to obtain a better fit to the experimental results.

CONSTITUTIVE MODELS AND MATERIAL PARAMETERS

In order to achieve a good compromise between simplicity and accuracy, a biaxial concrete model that provides acceptable representation of the cyclic inelastic behaviour of reinforced concrete under cyclic loading was used. This model (Merabet and Reynouard, 1999) adopts the concept of a smeared crack approach with a possible double cracking only at 90^0. It is based upon the plasticity theory for uncracked concrete with isotropic hardening and associated flow rule. Two distinct criteria describe the failure surface: Nadai in compression and bi-compression and Rankine in tension. Hardening is isotropic and an associated flow rule is used. When the ultimate surface is reached in tension, a crack is created perpendicularly to the principal direction of maximum tensile stress, and its orientation is considered as fixed subsequently. Each direction is then processed independently by a cyclic uniaxial law, and the stress tensor in the local co-ordinate system defined by the direction of the cracks is completed by the shear stress, elastically calculated with a reduced shear modulus μG, (with $0 < \mu < 1$, and μ being a function of the crack-opening strain) to account for the effect of interface shear transfer:

$\mu = 0.4$ ..... if $\varepsilon_{cr} - \varepsilon_{res} - \varepsilon_{tm} \le 2\varepsilon_{tm}$

$\mu = 0$ ..... if $\varepsilon_{cr} - \varepsilon_{res} - \varepsilon_{tm} \ge 2\varepsilon_{tm}$

$\mu = 0$ and $\sigma_{12} = 0$ ..... if $\varepsilon_{cr} - \varepsilon_{res} - \varepsilon_{tm} \ge 4\varepsilon_{tm}$

where:

ε_{cr} - total strain

ε_{res} - residual strain after unloading in compression

ε_{tm} - crack opening strain

σ_{12} - shear stress

The behaviour of a point initially under tension, which completely cracks prior to undergoing a reverse loading in compression, is illustrated in Figure 8. Similar laws describe the case of an initial compressed point or that of a point, which has not totally cracked under a reverse loading. The model has been described in detail and verified elsewhere (Ile, 2000; Ile and Reynouard, 2000; Fleury, 1996).

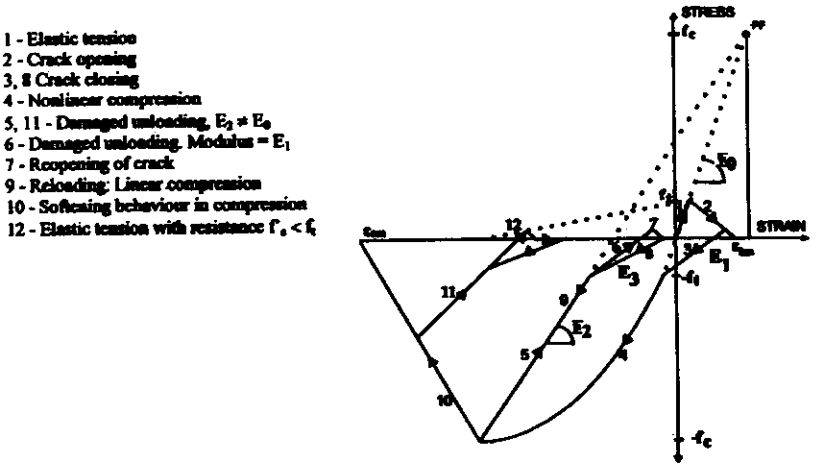

Fig. 8 Uniaxial model: point initially in tension

For steel, a cyclic model that can take into account the Bauschinger effect and buckling of reinforcing bars has been adopted. The monotonic branch is characterized by an initial linear branch followed by a plateau and hardening up to failure. The cyclic behaviour is described by the formulation proposed by Giuffré and Pinto and implemented by Menegoto and Pinto (1973). The steel model is presented in Figure 9.

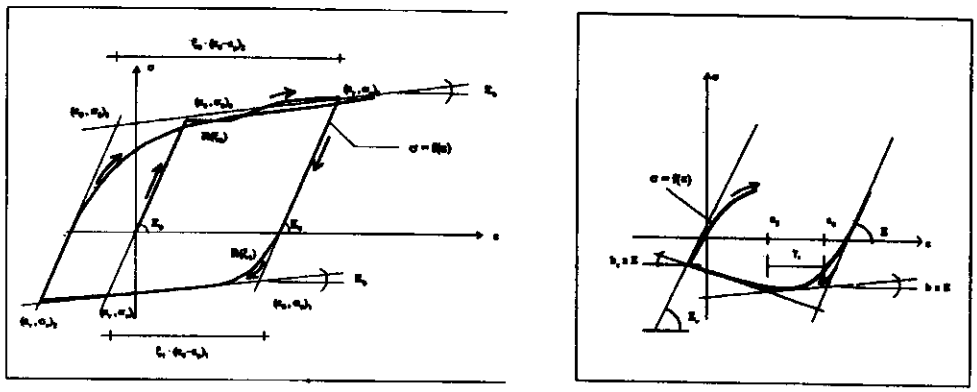

a) cyclic behaviour without buckling b) cyclic behaviour with buckling

Fig. 9 Numerical model for steel under cyclic loading

The bond behaviour under alternating loading is described through the law proposed by Eligehausen et al. (1983) and implemented by Fleury (1996) in the CASTEM 2000 code. The characteristics of the law are illustrated in Figure 10, in which a typical cycle (corresponding to a well-confined region) is shown. The behaviour under a monotonic load is described by the curve OABCD or $OA_1B_1C_1D_1$ and is entirely defined by the knowledge of s_1, s_2, s_3, τ_1, τ_3 and α. This curve is composed of four segments:

a non-linear ascending branch, its equation being given by $\tau = \tau_1.(s/s_1)^{\alpha}$,

the ascending branch is followed by a plateau for $s \in [s_1, s_2]$, defined for $\tau = \tau_1$.

a descending branch which is linear up to point C of co-ordinates (s_3, τ_3),

the last segment which defines the friction plateau, $\tau = \tau_3$.

The cyclic behaviour of the steel concrete interface is described in detail elsewhere (Fleury, 1996), and is not detailed here for the sake of brevity.

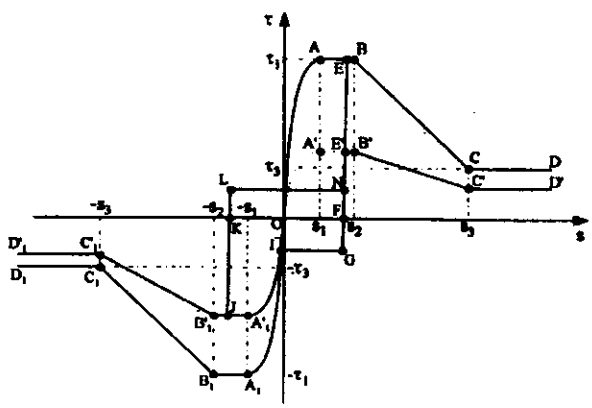

Fig. 10 Cyclic bond law

The evaluation of steel parameters was quite simple: the measured elasticity modulus, yield and failure stress being directly used (Fouré, 1998; Combescure, 1999). For concrete, the material properties were generally as provided by the CAMUS experimental data and design codes. Exceptionally, for

CAMUS III specimen, following the recommendations of EC8, the concrete compressive strength was increased from about 39 MPa to about 43 MPa in the confined regions. An initial value of 0.40 for the post-cracking parameter μ was assumed for all the three specimens. As bond test results on CAMUS II wall specimen were not available, the bond-slip parameters have been evaluated following the recommendations of CEB-FIP (1990) for smooth reinforcing steel. The parameters defining the bond-slip law were assumed as follows: $\tau_1 = \tau_3 = 1.5\,\text{MPa}$ and $s_1 = s_2 = s_3 = 0.1\,\text{mm}$.

COMPARISON WITH EXPERIMENTAL RESULTS

In the case of the first two specimens, the time history of the calculated roof displacement is compared in Figures 11 and 12 with the corresponding measured displacement. For the last specimen, this comparison (Figure 13) refers to the floor level 5, because transducers situated at floor level 6 were malfunctioning during the test. In each case, the comparisons are presented for a time interval where the horizontal displacements reach the most significant values. Despite the different reinforcement ratios used for the three walls and the relatively high level of the applied input motion, the agreement between numerical and experimental values, in all cases, is very acceptable.

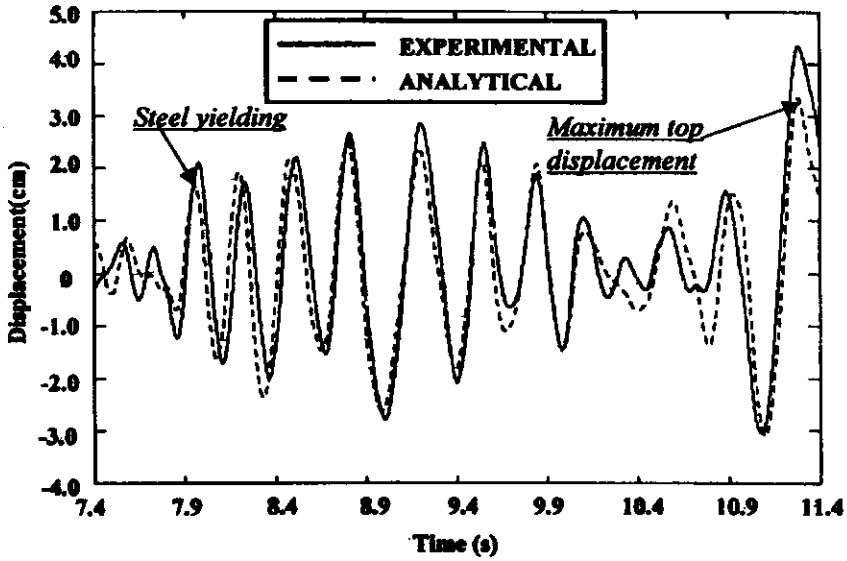

Fig. 11 Horizontal top displacement (floor level 6) (CAMUS I specimen)

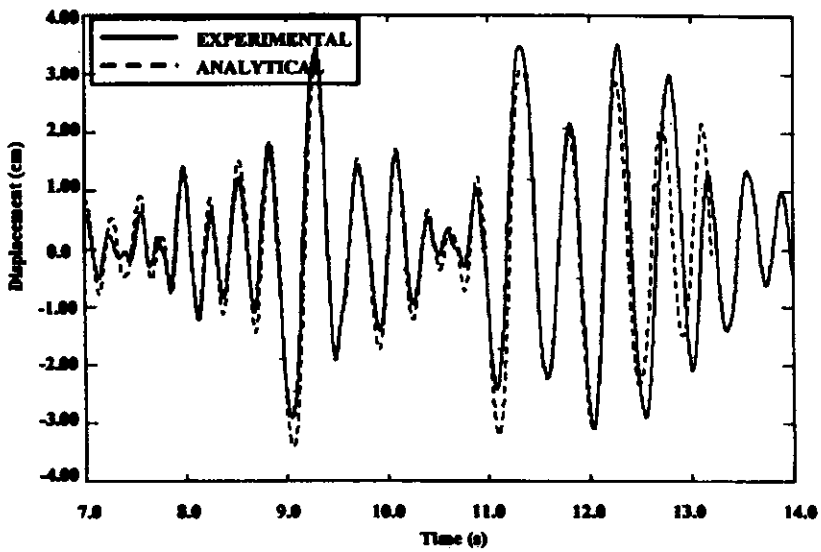

Fig. 12 Horizontal top displacement (floor level 6) (CAMUS II specimen)

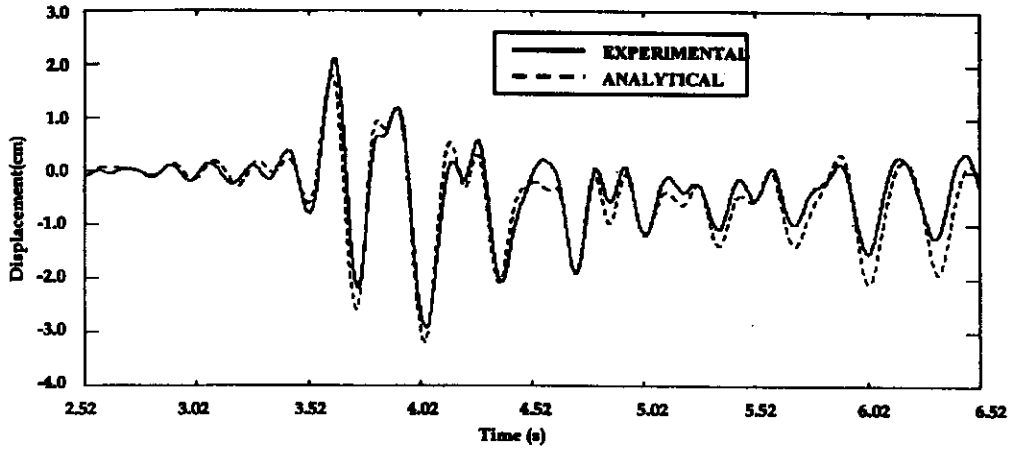

Fig. 13 Horizontal displacement (floor level 5) (CAMUS III specimen)

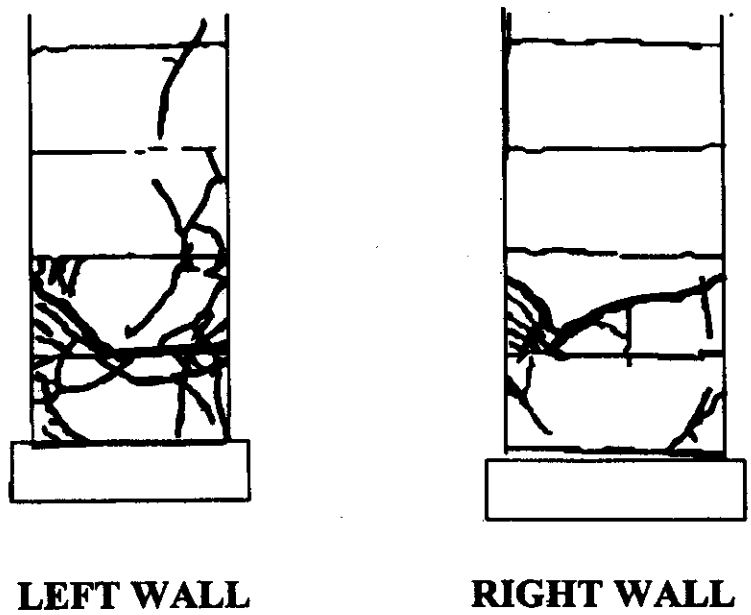

Fig. 14 Crack pattern of the CAMUS I specimen after the last test

Under the imposed horizontal motion, large inelastic deformations occur in the wall specimens. In the case of CAMUS I, although the design seismic level was 0.96g, the acceleration of the last test has been 0.71g. This is due to the failure pattern, which is quite different from that assumed in design. As can be seen clearly in Figure 14, the inclined crack patterns observed after the test are not consistent with the design which assumed horizontal cracks at each floor. However, numerical prediction of local damage, such as cracking, yielding of reinforcement and vertical strain profile show much more closer results to what has been experimentally observed. Local results as obtained from the dynamic analysis are seen in Figures 16 and 17. They depict the damage distribution obtained at the beginning of the steel-yielding (Figure 16) and at maximum displacement (Figure 17). It can be seen that when steel yielding takes place, developed cracks are almost horizontal and the deformed shape is similar to the first flexural mode. At the maximum displacement, however, damage is almost entirely concentrated at the level of the 2nd storey, and cracks previously formed at the curtailment of the flexural reinforcement tend to propagate in a diagonal direction. Hence, the failure mode indicated in Figures 16 and 17 is one of combined flexure and shear (tension shift), with shear inhibiting the development of the full flexural capacity after the formation of diagonal cracks. This situation is also depicted in Figure 15, where the bending moment-axial force interaction diagram at the critical section (at the 2nd storey, 10 cm below the inferior part of the floor) is

plotted, together with the variation of the axial load and moment as obtained experimentally during the failure test of CAMUS I specimen. The fact that some distance actually exists between (M,N) values and the envelope curve obtained by section analysis, seems to be an indication that bending moment capacity has been reduced due to the influence of shear. Visual inspection after the test showed that the steel bars were broken at the level of the interruption of steel bars (just below the 2nd floor level). All these observations indicate that the failure mode was more close to that involving a multiple lattice behaviour, while the design assumed horizontal cracks at each floor level (Coin, 1988). Therefore, the design method should be improved to take into account both potential failure mechanisms.

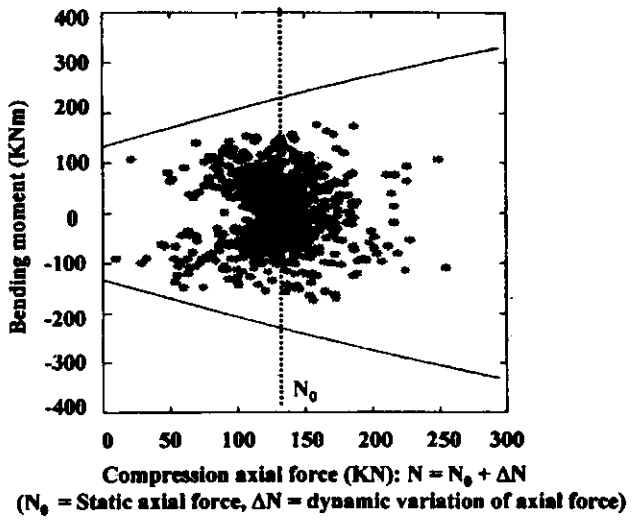

Fig. 15 Bending moment-axial force interaction diagram for CAMUS I

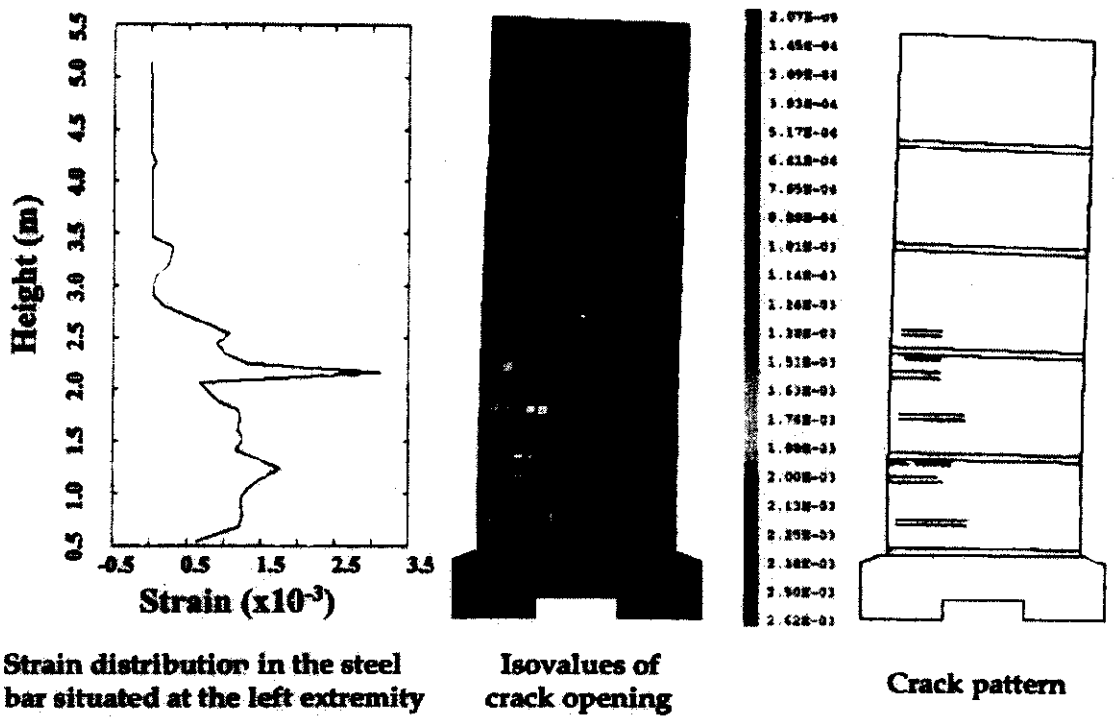

Fig. 16 Damage pattern for top displacement corresponding to steel-yielding (CAMUS I)

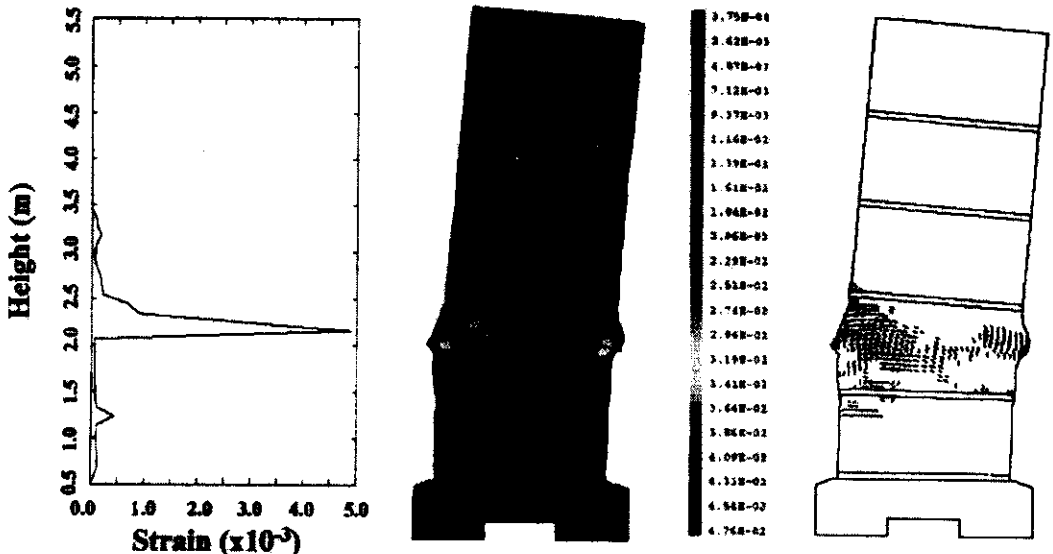

Fig. 17 Damage pattern for maximum top displacement (CAMUS I)

For the last test on CAMUS I, a large variation of the dynamic part of the axial force has equally been observed, its amplitude at the base of the 1st storey, being comparable with the static axial force which is about 163 KN for one wall. The first cause of this phenomenon is the extension mode due to bending: at maximum horizontal deflection, the neutral axis is at its maximum distance from the center of the wall cross-section, the raising of masses is maximum and the dynamic variation of the axial force is a tensile force; the frequency of this vertical motion is two times that of the horizontal movement (Bisch and Coin, 1998). The second reason of this phenomenon relies on the excitation of the first natural vertical mode of the system: at crack-closure, when concrete recovers its stiffness, compression forces strongly increase and these shocks excite the vertical vibration mode of the system (shaking table + specimen), which is at about 20 Hz (Sollogoub, 2000). Figure 18 shows a comparison between the experimental and predicted variations of the axial force at the base of the first storey. When comparing these results, it can be noted that the numerical results exhibit a clear difference in time, even though the maximum variation of the dynamic axial force is comparable. This indicates that it is more difficult to obtain a good match of the axial force variation as compared to the previously presented horizontal response quantities. One important parameter which may affect vertical response seems to be the value of the stiffness recovery at crack-closure in the concrete model. Although this aspect is not studied here, it deserves special attention and future research is needed.

Contrary to the CAMUS I specimen, the behaviour of the CAMUS II specimen was in accordance with the design: horizontal cracks developed at the level of the construction joints mainly at the base of the first and second storeys, and the applied acceleration level in the last test was 0.51g in comparison with the design level of 0.52g. Visual inspection of the specimen after the last test indicated that steel bars were broken at the base of the first storey and that they were buckled at the base of the second. Local results as obtained from the dynamic analysis are shown in Figure 19. It depicts the concrete strain profile corresponding to the maximum displacement reached at about 9.0 s during the last test (see Figure 12). It can be noted that the failure mechanism is characterized by widely-opened and in-phase horizontal cracks which are concentrated at the level of the construction joints. Due to the very low reinforcement ratio, the behaviour of this specimen is of a multi-block type, with rigid-block rotations of its different parts.

This behaviour is well depicted by the experimental and analytical moment-curvature relationships at the level of the 2nd construction joint shown in Figure 20. On one hand, these curves are very pinched and dissipated energy is not significant at this location. On the other hand, the variation of the axial force has a visible influence on the bending moment which clearly fluctuates in the plateau phase corresponding to steel-yielding. This indicates that the mechanism of resistance of such a very lightly reinforced wall has to

rely on the conversion of part of the seismic input energy to the potential energy needed for raising the masses. As observed in the case of the first specimen, the variation of the axial force due to the bending-induced oscillations is important and has to be accounted for in the design phase.

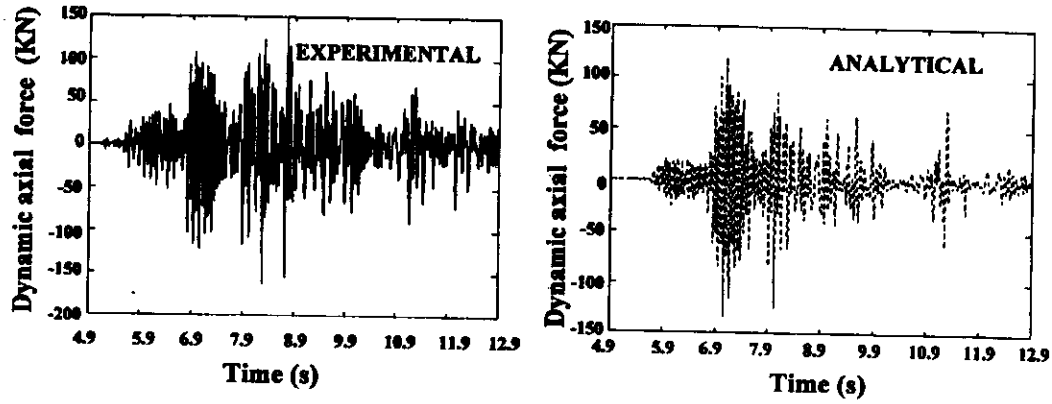

Fig. 18 Dynamic variation of the axial force at the base of the 1st storey

The seismic behaviour of the 3rd specimen (CAMUS III) was different from the previous ones. Being designed following the EC8 capacity design principles, this specimen was detailed to dissipate energy in a single flexural plastic hinge at the base. The Melendy Ranch (1.35g) test confirmed this intended behaviour, because essentially no flexural yielding occurred in the upper stories and damage was mainly concentrated in the first storey. A global pattern of the damage of the specimen after completion of the Melendy Ranch test as predicted by the numerical model, is shown in Figure 21. This figure shows the crack pattern and the vertical concrete strain profile corresponding to the maximum displacement response peak. For comparative purposes, the experimental crack pattern is presented in Figure 22. On examining the numerically predicted crack pattern, it can be observed that crack-directions do not always coincide with the experimental ones. It is to be noted, however, that in most problems, the overall behaviour of the wall and the general failure mechanism are more important than an accurate portrait of the crack pattern.

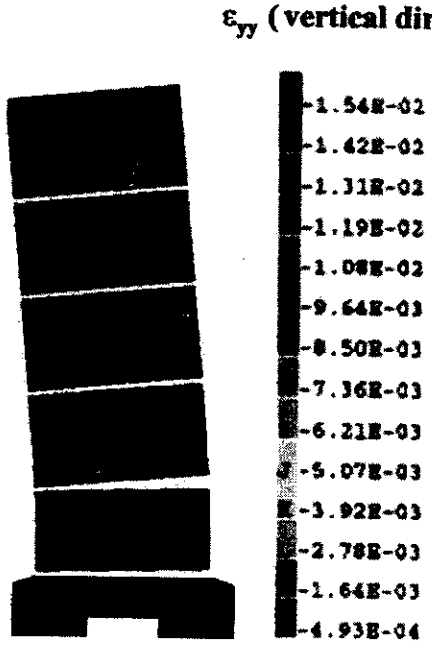

Fig. 19 Concrete strain profile for CAMUS II specimen at maximum top displacement

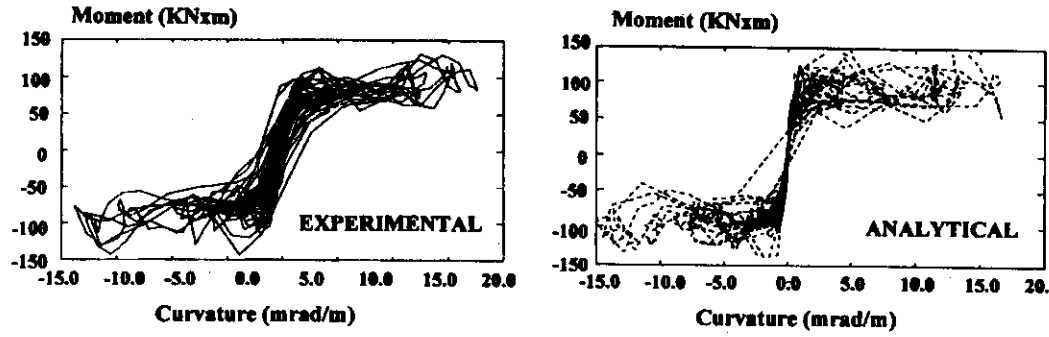

Fig. 20 Moment-curvature relationship at the base of the 2nd storey

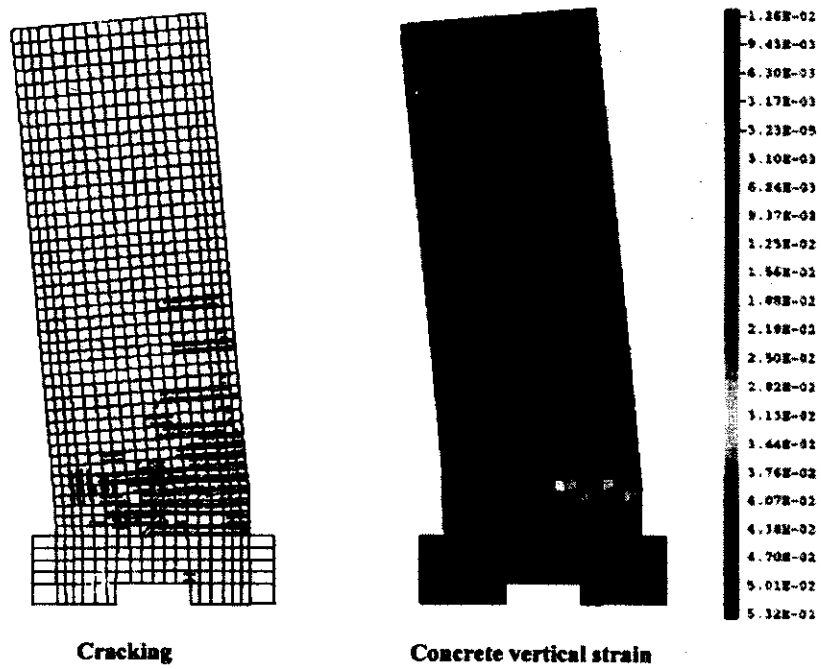

Fig. 21 Crack pattern and concrete strain profile for CAMUS III specimen at maximum top displacement (Melendy Ranch 1.35g test)

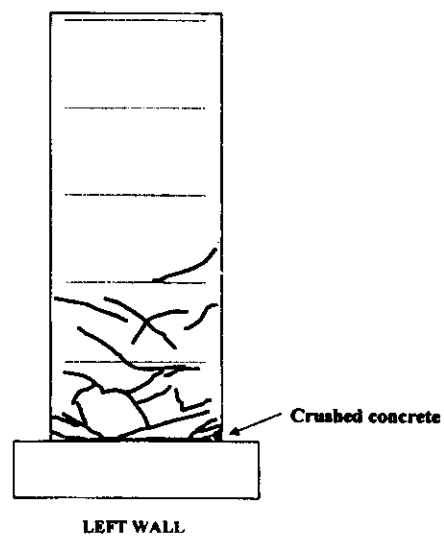

Fig. 22 Damage pattern of one wall at the end of the Melendy Ranch (1.35g) test

CONCLUSIONS

The present study of concrete walls subjected to seismic action has demonstrated the capability of the model to reproduce not only the main features of the global response, but also important details of the local behaviour. With respect to the lightly reinforced walls, the numerical model indicated different failure mechanisms, depending on the reinforcement ratio and detailing provisions. It is to be noted that a combined flexure and shear (tension shift) failure mode, as observed in the case of CAMUS I specimen, has not been accounted for in the design phase. The fact that this type of failure was reasonably predicted by the numerical results indicates that more interaction between design and non-linear analysis is needed. Design methods should also be improved to take into account the different potential behaviours observed during CAMUS I test. Due to its very low reinforcement ratio, the behaviour of the second specimen (CAMUS II) was of a multi-block type, indicating more clearly the principal features of the seismic behaviour of this type of structure: large horizontal cracks at each floor level and important variation of the axial force. Although the variation of the axial force is difficult to introduce in design, it has to be accounted for, because it may affect strain demand in the steel reinforcement (Bisch and Coin, 1998). Notwithstanding the complexity of the problem, it is to be noted that the only way to evaluate the range of variation of the axial force is to conduct non-linear analyses of the type already shown, taking into account the soil-structure interaction. The numerical results presented here were shown to be also effective in describing with sufficient accuracy the behaviour of a specimen designed following the EC8 capacity design principles. In accordance with its design, the predicted behaviour was that of a "ductile wall" developing a flexural plastic hinge at the base.

REFERENCES

1. ASCE (1982). "State-of-the-Art Report on Finite Element Analysis of Reinforced Concrete", ASCE Special Publication, New York, N.Y., U.S.A.
2. Bisch, P. and Coin, A. (1998). "The CAMUS Research", Proceedings of the 11th European Conference on Earthquake Engineering, Paris, France, Vol. 2.
3. Cafeel (2001). "Shear Walls" in Cafeel-Ecoest/Icons Thematic Report No. 5, (edited by J.M. Reynouard, and M.N. Fardis), LNEC.
4. CEB-FIP (1990). "Model-Code 1990", Bulletin d'information, Lausanne, Switzerland.
5. Coin, A. (1998). "Recherche CAMUS, Rapport Final, Démarche de l'ingénieur-Concepteur", Vols. 1 & 2, Ministère Francais de l'Equipement (Plan Genie Civil) Convention 9670011.
6. Combescure, D., Queval, J.C., Sollogoub, P., Bonnici, D. and Labbé, P. (1998). "Effect of Near-Field Earthquake on a R/C Bearing Wall Structure: Experimental and Numerical Studies", Proceedings of the 11th European Conference on Earthquake Engineering, Paris, France, Vol. 2.
7. Combescure, D. (1999). "CAMUS 3' International Benchmark, Report 1, Specimen and Loading Characteristics, Specifications for the Participants Report", Organized by CEA, EDF and GEO, under the Auspices of AFPS.
8. Eligehausen, R., Popov, E.P. and Bertero, V.-V. (1983). "Local Bond Stress-Slip Relationships of Deformed Base under Generalized Excitations", Report UCB/EERC-83/23, Earthquake Engg. Research Centre, Univ. of California, Berkeley, U.S.A.
9. EUROCODE 8 (1998). "Structures in Seismic Regions-Design, Part 1: General and Building", Report EUR 12266 EN, Office for Official Publications of the European Communities, Bruxelles, Belgium.
10. Fardis, M.N. (2000). "Eurocode 8 - Present State, Pre-normative and Co-normative Research Needs (including Design Seismic Action)", Proceedings of the Workshop: Mitigation of Seismic Risk Support to Recently Affected European Countries, European Commission-JRC, Belgirate (VB), Italy.
11. Fleury, F. (1996). "Prediction of the Behaviour of Reinforced Concrete Structures Subjected to Seismic Loading: Proposal for a Global Model for Beam Column Joints Integrating the Behaviour of Steel/Concrete Bond", Ph.D. Thesis, Blaise Pascal – Clermont II University, France.
12. Fouré, B. (1998). "Recherche CAMUS, Rapport Final, CEBTP, Matériaux, Contrôles, Examen de la Fissuration, ELU", Contribution du C.E.B.T.P., Dossier FNB 95 960, Ministère Français de l'Equipement (Plan Génie Civil) Convention 9670011.

13. Ile, N. (2000). "Behaviour of Reinforced Concrete Walls under Seismic Loading: Contribution Made by Experiment and Modelling to Design", Ph.D. Thesis, National Institute for Applied Sciences, Lyon, France.
14. Ile, N. and Reynouard, J.M. (2000). "Non-linear Analysis of Reinforced Concrete Shear Wall under Earthquake Loading", Journal of Earthquake Engineering, Vol. 4, No. 2, pp. 183-213.
15. Mazars, J. (1998). "French Advanced Research on Structural Walls: An Overview on Recent Seismic Programs", Proceedings of the 11th European Conference on Earthquake Engineering, Invited Lectures, Paris, France, pp. 21-41.
16. Menegoto, M. and Pinto, P. (1973). "Method of Analysis of Cyclically Loaded Reinforced Concrete Plane Frames including Changes in Geometry and Non-elastic Behaviour of Elements under Combined Normal Force and Bending", IABSE Symposium on Resistance and Ultimate Deformability of Structures Acted on by Well-Defined Repeated Loads, Final Report, Lisbon, Portugal.
17. Merabet, O. and Reynouard, J.M. (1999). "Formulation d'un Modèle Elasto-Plastique Fissurable Pour le Béton Sous Chargement Cyclique", Contract Study EDF/DER, Final Report, No. 1/943/002, URGC-Structures, National Institute for Applied Sciences, Lyon, France.
18. Millard (1993). "CASTEM 2000, Manuel d'utilisation", Report CEA-LAMBS No. 93/007, Saclay, France.
19. REGLES PS 92 (1995). "Règles de Construction Parasismique, Règles PS Applicables Aux Bâtiments, Dites Règles PS 92", Norme Française, AFNOR.
20. Sollogoub, P., Combescure, D., Queval, J.-C. and Chaudat, T. (2000). "In Plane Seismic Behaviour of Several 1/3rd Scaled R/C Bearing Walls – Testing and Interpretation Using Non-Linear Numerical Modelling", Proceedings of the 12WCEE Conference, Auckland, New Zealand.
21. Vulcano, A., Bertero, V.V. and Colotti, V. (1988). "Analytical Modeling of R/C Structural Walls", Proc. 9th WCEE, Vol. VI, Tokyo-Kyoto, Japan, pp. 41-46.